Mushroom-Type High-Impedance Surface With Loaded Vias: Homogenization Model and Ultra-Thin Design

Chandra S. R. Kaipa, *Student Member, IEEE*, Alexander B. Yakovlev, *Senior Member, IEEE*, Stanislav I. Maslovski, and Màrio G. Silveirinha, *Member, IEEE*

***Abstract*—In this letter, we study the reflection properties and natural modes (surface waves and leaky waves) of the mushroom-type surfaces with impedance loadings (as lumped loads) at the connection of the vias to the ground plane. The analysis is carried out using the nonlocal homogenization model for the mushroom structure with a generalized additional boundary condition for loaded vias. It is observed that the reflection characteristics obtained with the homogenization model strongly depend on the type of the load (inductive or capacitive) and are in a very good agreement with the full-wave simulation results. The proposed concept of lumped loads enables the design of an ultrathin mushroom-type surface with high-impedance resonance characteristics (zero reflection phase) for oblique incidence at low frequencies with a broad stopband for surface waves.**

***Index Terms*—Analytical modeling, electromagnetic band-gap (EBG) structures, high-impedance surface (HIS), homogenization, leaky waves, spatial dispersion (SD), surface waves, wire medium (WM).**

I. Introduction

SINCE the introduction of the mushroom-type electromagnetic band-gap (EBG) structure [1], hundreds of papers have been published exploring the theoretical challenges and practical realizations of such a type of high-impedance surface (HIS) due to their widespread applications in antenna technology and metamaterials. In general, mushroom-type HIS structures [formed by a grounded wire medium (WM) slab in conjunction with a capacitive grid] simultaneously (within the same frequency band) exhibit EBG properties associated with the stopband for surface waves and artificial magnetic conductor (AMC) properties related to the reflection phase behavior (typically when the phase varies in between $+90^\circ$ to -90°). Recent trends in the fast and accurate analysis techniques resulted in more sophisticated homogenization models that capture the physics of the plane-wave interaction [2] and surface-wave and leaky-wave propagation [3] on these structures. In general, the wire medium is characterized by a strong spatial dispersion (SD) at microwaves [4]. However, in [2] and [3], it has been shown that under some conditions, the SD effects can be significantly reduced in a mushroom HIS. More recently, structured WM slabs with impedance insertions in the vias have been studied in [5] and [6]. In [5], a WM slab connected to the ground plane through reactive loads is considered, demonstrating a strong dependence of the reflection characteristics on the value and type of the load. In [6], a WM slab with inductively loaded vias terminated by patches is shown to behave as a local uniaxial epsilon-negative (ENG) material with suppressed SD effects, consistent with a related proposal of [7].

This letter focuses on the reflection phase characteristics and surface-wave and leaky-wave propagation in the mushroom-type surfaces with vias connected to the ground plane through lumped loads. The analysis is carried out using the nonlocal homogenization model for the WM with the generalized additional boundary conditions (GABCs) derived in a quasi-static approximation by including arbitrary junctions with impedance insertions (as lumped loads) [5]. It is observed that with an increase in the value of the inductive load, there is a decrease in the plasma frequency with a reduction in the SD effects, which is consistent with the findings recently reported in [6]. Based on this concept of inductive loads, we show that it is possible to design an ultrathin structure that shifts the HIS resonances for obliquely incident transverse magnetic (TM) plane waves to lower frequencies, with a stopband for surface waves over the broad frequency range. The predictions of the homogenization model are in a very good agreement with the full-wave results.

II. Homogenization Model

The geometry of the mushroom structure considered in this letter is shown in Fig. 1. The structure is illuminated by a TM-polarized plane wave incident in the xz-plane at an angle θ_i. The wires with radius r_0 are directed along the z-direction in the host medium with permittivity $\varepsilon_{\rm h}$ and are connected to the patches at the plane $z = 0$ and to the ground plane through the lumped loads at the plane $z = -h$. The period of the square patches is a, and the gap between the patches is g.

The analysis is carried out using the nonlocal homogenization model [2], wherein the WM slab is modeled as a uniaxial continuous material characterized by a spatially dispersive effective

Manuscript received October 14, 2011; accepted December 10, 2011. Date of publication December 21, 2011; date of current version January 30, 2012.

C. S. R. Kaipa and A. B. Yakovlev are with the Department of Electrical Engineering, The University of Mississippi, University, MS 38677 USA (e-mail: ckaipa@olemiss.edu; yakovlev@olemiss.edu).

S. I. Maslovski and M. G. Silveirinha are with the Departamento de Engenharia Electrotécnica, Instituto de Telecomunicações, Universidade de Coimbra Pólo II, 3030-290 Coimbra, Portugal (e-mail: stas@co.it.pt; mario.silveirinha@co.it.pt).

Color versions of one or more of the figures in this letter are available online at http://ieeexplore.ieee.org.

Digital Object Identifier 10.1109/LAWP.2011.2180694

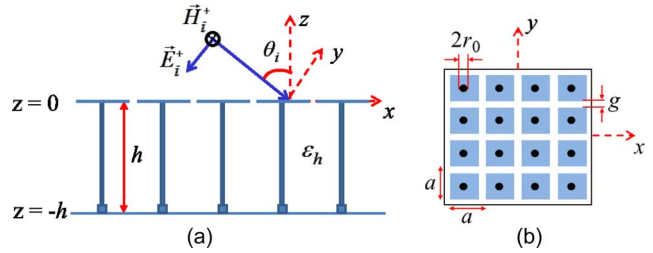

Fig. 1. Geometry of the mushroom structure with loads excited by an obliquely incident TM-polarized plane wave: (a) cross-section view and (b) top view.

dielectric function along the direction of wires: $\varepsilon_{zz} = \varepsilon_{\rm h}(1 - k_{\rm p}^2/(k_{\rm h}^2 - k_z^2))$, where $k_{\rm p} = \sqrt{(2\pi/a^2)/\log[a^2/4r_0(a-r_0)]}$ is the plasma wavenumber as defined in [9], $k_{\rm h} = k_0\sqrt{\varepsilon_{\rm h}}$ is the wavenumber in the host medium, $k_0 = \omega/c$ is the free-space wavenumber, and k_z is the z-component of the wave vector $\mathbf{k}$ inside the material.

A TM-polarized incident wave excites TM and transverse electromagnetic (TEM) waves in the WM slab, and the corresponding magnetic fields in the air and the wire-medium region can be expressed as

$$\begin{aligned} H_y|_{z>0} &= e^{\gamma_0 z} - \rho e^{-\gamma_0 z} \\ H_y|_{z<0} &= A_{\rm TM}^{+} e^{\gamma_{\rm TM}(z+h)} + A_{\rm TM}^{-} e^{-\gamma_{\rm TM}(z+h)} \\ &\quad + B_{\rm TEM}^{+} e^{\gamma_{\rm TEM}(z+h)} + B_{\rm TEM}^{-} e^{-\gamma_{\rm TEM}(z+h)} \end{aligned} \quad (1)$$

where $\gamma_0 = \sqrt{k_x^2 - k_0^2}$, $\gamma_{\rm TM} = \sqrt{k_{\rm p}^2 + k_x^2 - k_0^2\varepsilon_{\rm h}}$, $\gamma_{\rm TEM} = jk_{\rm TEM} = jk_0\sqrt{\varepsilon_{\rm h}}$, and $k_x = k_0 \sin\theta_i$ is the x-component of the wave vector $\mathbf{k}$. The field amplitudes $A_{\rm TM}^{\pm}$, $B_{\rm TEM}^{\pm}$, and the reflection coefficient ρ are to be determined by enforcing appropriate boundary conditions. Apart from the two-sided impedance boundary condition at the air-patch interface and the classical boundary condition at the ground plane, additional boundary conditions are required at each wire termination due to the nonlocal response of the wire medium.

Following [5], the discontinuities in the microscopic wire current distribution $I(z)$ at the connections of the wires to the patches and to the ground plane through lumped loads are taken into account through the following GABCs:

$$\left[\frac{dI(z)}{dz} + \left(\frac{C}{C_{\rm patch}}\right) I(z)\right]_{z=0} = 0 \quad (2)$$

$$\left[\frac{dI(z)}{dz} - (j\omega C Z_{\rm Load}) I(z)\right]_{z=-h} = 0 \quad (3)$$

where C is the capacitance per unit length of the wire medium, $C_{\rm patch}$ is the capacitance of the patch in a regular array of patches defined in [8], and $Z_{\rm Load}$ is the impedance of the lumped load. The microscopic wire current can be expressed in terms of the bulk electromagnetic fields as $I(z) = -ja^2[(k_0\varepsilon_{\rm h}/\eta_0)E_z + k_x H_y]$. Since the insertion of loads in the wire introduces nonuniformity in the current and charge distributions, the correction terms such as the parasitic capacitance $C_{\rm par}$ and parasitic inductance $L_{\rm par}$ should be taken into account for the load impedance in (3) [5]

$$Z_{\rm Load,eff} = j\omega L_{\rm par} + \frac{1}{j\omega C_{\rm par} + (1/Z_{\rm Load})}. \quad (4)$$

Now, applying the classical boundary condition, two-sided impedance boundary condition, and the GABCs [(2) and (3)], the reflection coefficient can be expressed as follows:

$$\rho = \frac{(jk_0 - \eta_0\gamma_0 Y_g)K - jk_0\gamma_0 M}{(jk_0 + \eta_0\gamma_0 Y_g)K + jk_0\gamma_0 M} \quad (5)$$

where $Y_g = j(\varepsilon_{\rm h}+1)(k_0 a/\eta_0\pi)\log[\csc(\pi g/2a)]$ is the grid admittance of the patch array given in [10]

$$\begin{aligned} K &= \gamma_{\rm TM}\sinh(\gamma_{\rm TM}h)\cos(k_{\rm TEM}h) - k_{\rm TEM}\sin(k_{\rm TEM}h) \\ &\quad \times \left[\left(\frac{\varepsilon_{\rm h}}{\varepsilon_{zz}^{\rm TM}} - 1\right)\cosh(\gamma_{\rm TM}h) + \frac{\varepsilon_{\rm h}\gamma_{\rm TM}\sinh(\gamma_{\rm TM}h)}{\varepsilon_{zz}^{\rm TM} j\omega C Z_{\rm Load,eff}}\right] \end{aligned} \quad (6)$$

and

$$\begin{aligned} M &= 2\left(\varepsilon_{\rm h} - \varepsilon_{zz}^{\rm TM}\right) \\ &\quad + \cosh(\gamma_{\rm TM}h)\left[\frac{j\varepsilon_{\rm h}k_{\rm TEM}}{\omega C Z_{\rm Load,eff}}\sin(k_{\rm TEM}h) \right. \\ &\quad \left. + \left(\varepsilon_{\rm h}\left(\frac{\varepsilon_{\rm h}}{\varepsilon_{zz}^{\rm TM}} - 2\right) + 2\varepsilon_{zz}^{\rm TM}\right)\cos(k_{\rm TEM}h)\right] \\ &\quad + \left(\varepsilon_{\rm h} - \varepsilon_{zz}^{\rm TM}\right)\sinh(\gamma_{\rm TM}h) \\ &\quad \times \left[\left(\frac{\gamma_{\rm TEM}}{\gamma_{\rm TM}} + \frac{\gamma_{\rm TM}}{\gamma_{\rm TEM}}\right) j\sin(k_{\rm TEM}h) \right. \\ &\quad \left. + \frac{\varepsilon_{\rm h}\gamma_{\rm TM}}{\varepsilon_{zz}^{\rm TM} j\omega C Z_{\rm Load,eff}}\cos(k_{\rm TEM}h)\right]. \end{aligned} \quad (7)$$

Here, $\varepsilon_{zz}^{\rm TM} = \varepsilon_{\rm h}k_x^2/(k_p^2 + k_x^2)$ is the relative effective permittivity along the direction of the vias for TM polarization. In Section III, the predictions of the homogenization model are described together with the full-wave results.

III. Results and Discussion

We consider the case of a mushroom structure with the vias connected to the ground plane through lumped loads. The dimensions of the structure (with the notations as shown in Fig. 1) are as follows: $a = 2$ mm, $g = 0.2$ mm, $r_0 = 0.05$ mm, $h = 1$ mm, $\varepsilon_{\rm h} = 10.2$, and $\theta_i = 60°$. Fig. 2 demonstrates the reflection phase characteristics for different lumped loads as a function of frequency. In the full-wave simulations, it is assumed that the load is connected to the ground plane through a gap of 0.1 mm. By comparing the analytical results with the full-wave results using HFSS [11], it is estimated (by curve fitting) that the gap is characterized by the parasitic capacitance $C_{\rm par} \approx 0.02$ pF and parasitic inductance $L_{\rm par} \approx 0.06$ nH. It can be seen that the homogenization results are in a good agreement with the full-wave numerical results. It can be observed that the reflection phase (with the HIS resonances, corresponding to the reflection phase of 0° and 360°) depends strongly on the value and on the type of the load. It is important to point out that with an increase of the reactance of the inductive load, the HIS resonance shifts to lower frequencies, which is related to the decrease in the plasma frequency accompanied with a reduction of SD effects [6].

Next, we study the natural modes of the mushroom structure based on the numerical solution of the dispersion equation (denominator of the reflection coefficient) (5) as a root search for the complex propagation constant k_x. In Fig. 3, we plot

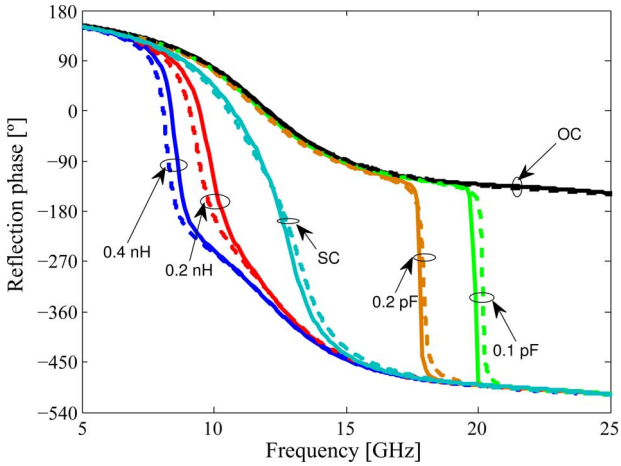

Fig. 2. Phase of the reflection coefficient as a function of frequency for the mushroom structure with vias connected to the ground plane through inductive loads ($L = 0.2$ nH and 0.4 nH), capacitive loads ($C = 0.1$ pF and 0.2 pF), short circuit (SC), and open circuit (OC) excited by a TM-polarized plane wave incident at $\theta_i = 60°$. The dotted lines represent the analytical results, and the solid lines correspond to the simulations results obtained using HFSS.

the dispersion behavior of the normalized phase and attenuation constants of the TM^x surface-wave and leaky-wave modes of the mushroom structure with an inductive load of 0.4 nH. The homogenization results are in good agreement with the CST [12] results for the proper forward and backward TM^x surface-wave modes. Also in Fig. 3, the results with a true short circuit (SC) at the connection of the vias to the ground plane (light-colored lines) are shown, which are qualitatively consistent with [3, Fig. 19]. It can be observed that the dispersion curves in the case of 0.4 nH load are shifted to lower frequencies in comparison to the SC case studied in [3]. From Fig. 3, the stopband for the TM^x surface-wave modes is from 7.54 to 8.74 GHz. The lower band edge (7.54 GHz) corresponds to the frequency at which the propagation of first proper bound mode stops (the phase velocities of the forward and backward modes are equal), and the upper band edge (8.74 GHz) corresponds to the cutoff frequency of the second proper (forward) TM^x surface-wave mode, which propagates above the plasma frequency. It is observed that the AMC bandwidth 7.61–8.28 GHz (calculated for 60° incidence) coincides with the stopband for the surface waves. In Fig. 3, it can be seen that the propagation constant of the proper complex mode approaches zero at the plasma frequency of 8.4 GHz. The percentage decrease in the plasma frequency when compared to the mushroom structure with SC vias is nearly 31%. Thus, using the inductive loads, we can effectively shift the HIS properties (EBG and AMC) of the mushroom structure to lower frequencies for TM-polarized waves. With this type of loading, it is possible to design very compact structures with miniaturized unit cells (i.e., electrical length of the unit cell being much smaller than the wavelength) at the frequency of operation.

Next, we consider the case of the air-filled mushroom structure (with the same structural dimensions as used in the calculations in Fig. 2) utilizing inductive loads of a large value in order to achieve an ultrathin design with better AMC and EBG properties. The homogenization results of the reflection phase characteristics are compared to the HFSS results in Fig. 4,

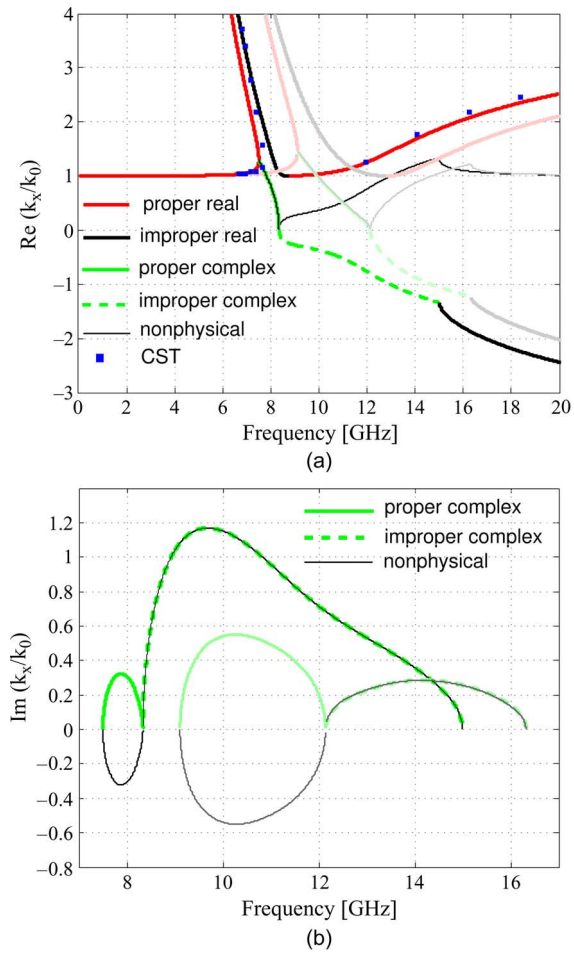

Fig. 3. Dispersion behavior of TM^x surface-wave and leaky-wave modes in the mushroom structure with an inductive load of 0.4 nH: (a) normalized phase constant and (b) normalized attenuation constant. The light-colored lines correspond to the case with SC vias.

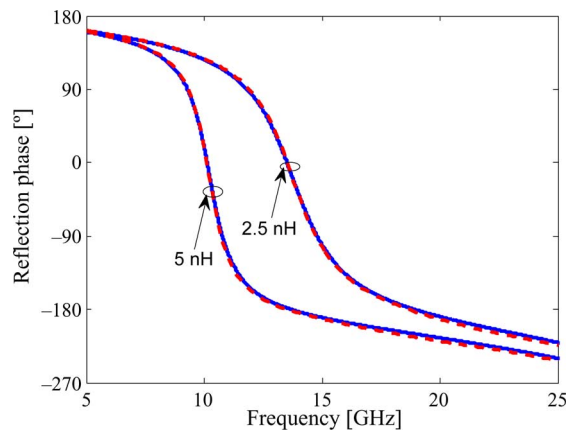

Fig. 4. Phase of the reflection coefficient as a function of frequency for the mushroom structure with the vias connected to the ground plane through inductive loads ($L = 2.5$ nH and 5 nH) excited by a TM-polarized plane wave incident at $\theta_i = 45°$. The solid lines represent the homogenization model results, and the dotted lines correspond to the full-wave HFSS results.

showing a near perfect agreement. The effects of the parasitic inductance and parasitic capacitance are negligible in this configuration. It can be observed from Fig. 4 that the HIS resonances (corresponding to the reflection phase of 0°) for the 45°

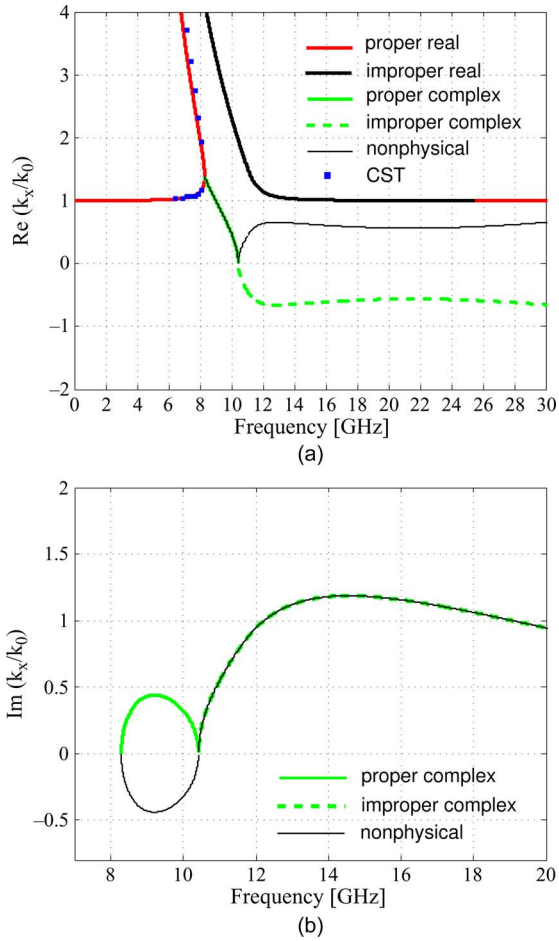

Fig. 5. Dispersion behavior of TM^x surface-wave and leaky-wave modes in the air-filled mushroom structure with an inductive load of 5 nH: (a) normalized phase constant and (b) normalized attenuation constant.

TM-polarized plane-wave incidence are at 10.1 GHz (for 5-nH load) and 13.5 GHz (for 2.5-nH load). These resonances are significantly shifted to lower frequencies when compared to the structure without loads, which resonates at 25 GHz. It should be noted that this shift in the resonances is only observed for obliquely incident TM plane waves. However, for normal incidence and also for transverse electric (TE) plane waves, which do not interact with the vias, the HIS resonance occurs at significantly higher frequencies (around 26 GHz). The electrical thickness of the structure for 5-nH load is approximately $\lambda/30$ at the operating frequency. An interesting observation is that the second HIS resonance (usually seen in a typical mushroom surface) is shifted to higher frequencies when large inductive loads are used.

The dispersion behavior of the normalized phase and attenuation constants of the TM^x surface-wave and leaky-wave modes of the air-filled mushroom structure with 5-nH load predicted by the analytical model is shown in Fig. 5 and compared to CST results, showing a good agreement for the proper forward and backward TM^x surface-wave modes. One may notice a wide stopband for the surface-wave modes, which is over a broad frequency range from 8.29 to 25.51 GHz. The cutoff frequency of the second proper TM^x surface-wave mode is far above the plasma frequency of 10.42 GHz (as can be seen in Fig. 5, the propagation constant of the proper complex mode approaches zero). The percentage reduction in the plasma frequency when compared to the structure without loads is nearly 73%.

IV. Conclusion

The reflection phase characteristics and the surface-wave and leaky-wave propagation in the loaded mushroom structure have been studied using the nonlocal homogenization model with generalized ABCs at the insertion of impedance loadings and are validated against the full-wave results. It is observed that the reflection phase depends strongly on the value and type (inductive or capacitive) of the load impedance. The proposed concept on lumped loads may enable to design more compact and tunable mushroom structures, which find applications in antenna technology and in the design of ultrathin absorbers. As an example, we have outlined the design of an ultrathin mushroom-type surface with a wide stopband for surface-wave propagation, which may find application in the design of ridge gap waveguides.

References

[1] D. Sievenpiper, L. Zhang, R. F. J. Broas, N. G. Alexopoulos, and E. Yablonovich, "High-impedance electromagnetic surfaces with a forbidden frequency band," *IEEE Trans. Microw. Theory Tech.*, vol. 47, no. 11, pp. 2059–74, Nov. 1999.

[2] O. Luukkonen, M. G. Silveirinha, A. B. Yakovlev, C. R. Simovski, I. S. Nefedov, and S. A. Tretyakov, "Effects of spatial dispersion on reflection from mushroom-type artificial impedance surfaces," *IEEE Trans. Microw. Theory Tech.*, vol. 57, no. 11, pp. 2692–2699, Nov. 2009.

[3] A. B. Yakovlev, M. G. Silveirinha, O. Luukkonen, C. R. Simovski, I. S. Nefedov, and S. A. Tretyakov, "Characterization of surface-wave and leaky-wave propagation on wire-medium slabs and mushroom structures based on local and nonlocal homogenization models," *IEEE Trans. Microw. Theory Tech.*, vol. 57, no. 11, pp. 2700–2714, Nov. 2009.

[4] P. A. Belov, R. Marqués, S. I. Maslovski, I. S. Nefedov, M. Silveirinha, C. R. Simovski, and S. A. Tretyakov, "Strong spatial dispersion in wire media in the very large wavelength limit," *Phys. Rev. B*, vol. 67, p. 113103, 2003.

[5] S. I. Maslovski, T. A. Morgado, M. G. Silveirinha, C. S. R. Kaipa, and A. B. Yakovlev, "Generalized additional boundary conditions for wire media," *New J. Phys.*, vol. 12, p. 113047, 2010.

[6] C. S. R. Kaipa, A. B. Yakovlev, S. I. Maslovski, and M. G. Silveirinha, "Indefinite dielectric response and all-angle negative refraction in a structure with deeply-subwavelength inclusions," *Phys. Rev. B*, vol. 84, p. 165135, 2011.

[7] A. Demetriadou and J. B. Pendry, "Taming spatial dispersion in wire metamaterial," *J. Phys., Condens. Matter*, vol. 20, p. 295222, 2008.

[8] S. I. Maslovski and M. G. Silveirinha, "Nonlocal permittivity from a quasistatic model for a class of wire media," *Phys. Rev. B*, vol. 80, p. 245101, 2009.

[9] S. A. Tretyakov, *Analytical Modeling in Applied Electromagnetics*. Boston, MA: Artech House, 2003.

[10] O. Luukkonen, C. Simovski, G. Granet, G. Goussetis, D. Lioubtchenko, A. V. Räisänen, and S. A. Tretyakov, "Simple and accurate analytical model of planar grids and high-impedance surfaces comprising metal strips or patches," *IEEE Trans. Antennas Propag.*, vol. 56, no. 6, pp. 1624–1632, Jun. 2008.

[11] HFSS: High Frequency Structure Stimulator based on finite element method. ver. 12, Ansoft Corporation, Canonsburg, PA [Online]. Available: http://www.ansoft.com

[12] CST Microwave Studio CST GmbH, Darmstadt, Germany, 2011 [Online]. Available: http://www.cst.com